Nuclear Instruments and Methods in Physics Research A 749 (2014) 19–26

Contents lists available at ScienceDirect

Nuclear Instruments and Methods in Physics Research A

journal homepage: www.elsevier.com/locate/nima

γ-Particle coincidence technique for the study of nuclear reactions

V.A.B. Zagatto [a,*], J.R.B. Oliveira [a], P.R.P. Allegro [a], L.C. Chamon [a], E.W. Cybulska [a], N.H. Medina [a], R.V. Ribas [a], W.A. Seale [a], C.P. Silva [a], L.R. Gasques [a], G.S. Zahn [b], F.A. Genezini [b], J.M.B. Shorto [b], J. Lubian [c], R. Linares [c], D.L. Toufen [d], M.A.G. Silveira [e], E.S. Rossi Jr. [f], G.P. Nobre [g]

[a] Instituto de Física da Universidade de São Paulo, Brazil
[b] Instituto de Pesquisas Energéticas e Nucleares, Brazil
[c] Instituto de Física da Universidade Federal Fluminense, Brazil
[d] Instituto Federal de Educação, Ciência e Tecnologia, Brazil
[e] Centro Universitário da FEI, Brazil
[f] Centro Universitário FIEO – UNIFIEO, Brazil
[g] Lawrence Livermore National Laboratory, United States

ARTICLE INFO

Article history:
Received 13 August 2013
Received in revised form
5 February 2014
Accepted 6 February 2014
Available online 22 February 2014

Keywords:
γ-Ray spectrometer
γ-Particle coincidence
Inelastic reactions

ABSTRACT

The Saci-Perere γ ray spectrometer (located at the Pelletron AcceleratorLaboratory – IFUSP) was employed to implement the γ-particle coincidence technique for the study of nuclear reaction mechanisms. For this, the $^{18}O + ^{110}Pd$ reaction has been studied in the beam energy range of 45–54 MeV. Several corrections to the data due to various effects (energy and angle integrations, beam spot size, γ detector finite size and the vacuum de-alignment) are small and well controlled. The aim of this work was to establish a proper method to analyze the data and identify the reaction mechanisms involved. To achieve this goal the inelastic scattering to the first excited state of ^{110}Pd has been extracted and compared to coupled channel calculations using the São Paulo Potential (PSP), being reasonably well described by it.

1. Introduction

The Saci-Perere γ-ray spectrometer [1] was originally designed for nuclear structure studies with fusion reactions followed by the evaporation of protons and α particles. The good energy resolution of γ-ray detectors allows the identification of close lying states, populated in nuclear reactions, by γ-particle coincidence measurements. This characteristic may be used to measure nuclear reactions, focusing on the study of reaction mechanisms such as inelastic scattering, transfer, inelastic break-up and fusion (complete and incomplete). The main objective of this work is to implement a technique that allows us to measure different scattering angular distributions using the γ-spectrometer *Saci-Perere*. This upgrade converted the spectrometer into a useful tool which allows different studies in varied areas of nuclear physics using a single instrument. The advantage of using this particular spectrometer consists in its ancillary system composed by eleven plastic phoswich scintillators that allow measurements at eleven different scattering angles at the same time.

Typical Si detectors can get degraded with high count rates of heavy ions. In the case of the present γ-particle coincidence experiment a high count rate ($> 10^4$ Hz) is necessary to compensate for the low efficiency of the γ-ray detectors. However, the excellent γ-ray energy resolution allows the identification of the populated states in most cases and a good particle detector resolution is not necessary. Due to this fact, despite having worse resolution than Si detectors, it was decided to use plastic phoswich scintillator detectors. Another fact that accounts for the use of plastic particle detectors, besides their radiation hardness, is their low cost compared to Si detectors.

The disadvantages of this method are the fact that reactions with no γ decay cannot be measured and the necessity to evaluate several corrections to the data in order to obtain the absolute differential cross-sections. Such corrections arise mainly from the indirect population of states by γ decay, from the γ-ray anisotropy, and from the difficulty in the evaluation of the vacuum de-alignment effect (for further information see Chapter 2 of Ref. [2]). This introduction is followed by the description of the experimental setup and procedure. The data reduction is explained in Section 3, giving special attention to the analysis of γ-particle coincidences. Then, the extraction of the differential cross-sections from the experimental yields is described, showing how the different corrections may change the angular

* Corresponding author.
E-mail address: vinicius.zagatto@gmail.com (V.A.B. Zagatto).

http://dx.doi.org/10.1016/j.nima.2014.02.014
0168-9002

distribution of the γ decay. Finally, the results and conclusions are expressed.

2. Experimental setup

The Saci-Perere (acronym for *Sistema Ancilar de Cintiladores – Pequeno Espectrômetro de Radiação Eletromagnética com Rejeição de Espalhamento*) is a system which consists of four HPGe detectors (two of 60% and two of 20% efficiency relative to a 3 in. × 3 in. NaI (Tl) scintillator detector) coupled to BGO Compton suppressors for γ-ray measurements and an ancillary system of eleven Δ*E*–*E* plastic phoswich scintillators (solid angle coverage of 76% of 4π) for particle measurements. Table 1 presents the angle between the direction of each of the HPGe detectors and the direction of the incident beam (polar angle – θ) and the corresponding azimuthal angle (ϕ) relative to the horizontal plane.

To adapt the system for nuclear reaction studies it was necessary to reduce the solid angle of each detector to limit the count rate (in the forward detectors) or the scattering angle range (for the backward angle detectors). This was achieved with a set of Al plates with collimating holes placed on the face of each particle detector. Due to the fact that different scattering angles have different count rates, the number and the diameter of the holes must be different for each detector. Table 2 presents the angular positions (spherical coordinates) and solid angles delimitated by each collimating hole, while Fig. 1 shows the set of Al collimators used in the experiment.

The $^{18}O+^{110}Pd$ reaction was measured with this setup in two separate experiments with beam energies of 45.4, 50.1 and 53.6 MeV provided by the Pelletron-8 UD Tandem Accelerator, at

Table 1
Table showing the polar (θ) and azimuthal angle (ϕ) of each γ-ray detector, respectively.

Detector	θ (°)	ϕ (°)
G1	37	180
G2	101	0
G3	101	35.3
G4	37	20.9

Table 2
Table showing the polar (θ) and azimuthal angles (ϕ) of each collimating aperture and its solid angle ($\Delta\Theta$ in msr). The first column refers to the number of the particle detector. The largest scattering angle detectors have more than one aperture (up to three) at about the same azimuthal angle. The angles were measured after the manufacture of the pieces and the uncertainty associated will be explained in Section 5.

Detector	θ (°)	ϕ (°)	$\Delta\Theta$ (msr)
C1	30	0	0.64
C2	43	108	2.00
C3	53	36	2.72
C4	65	324	4.71
C5	71	252	6.78
C6	80	180	8.67
C7	99	8	8.63
C7	99	353	8.50
C8	107	297	14.96
C8	108	282	15.21
C9	118	234	16.68
C9	116	217	15.91
C9	117	199	16.10
C10	127	164	24.69
C10	126	146	24.49
C10	129	130	25.51
C11	135	94	37.84
C11	136	74	38.32
C11	138	55	38.97

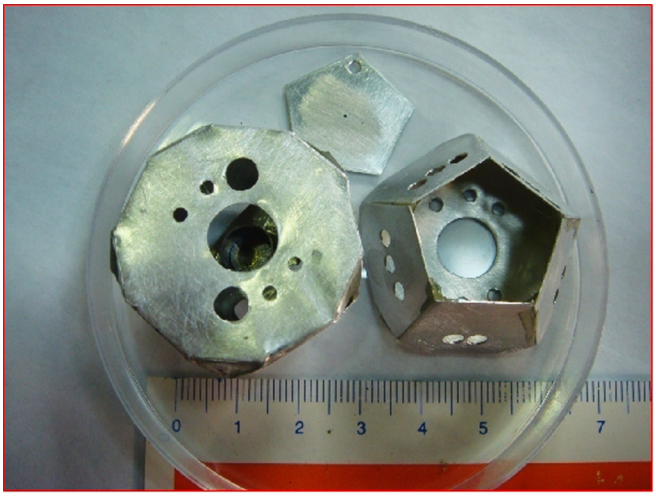

Fig. 1. Set of Al collimators used in the forward (left) and backward (right) hemisphere detectors.

the "Instituto de Física da Universidade de São Paulo". The ^{18}O beam was extracted at the ion source from a lithium hydroxide cathode sample. The enriched (>97%) ^{110}Pd isotope target had a thickness of 0.84 mg/cm^2 with an Au backing thickness of 1.49 mg/cm^2. To study the effects of γ-ray decay of the recoiling nucleus in flight, the target was turned around, so, the ^{18}O beam traversed the Au layer before hitting the Pd target. The Au backing has no function in the present experiment. Its presence is due to the fact that this target was originally used for nuclear structure experiments. The ^{18}O beam is easily obtained at the Pelletron accelerator with high intensity. The $^{18}O+^{110}Pd$ reaction makes it possible to study the 2n transfer reaction (forming ^{112}Pd) and the inelastic scattering to the first excited state of ^{110}Pd, among other processes. For the experiments, the electronic and data acquisition system was configured for γ-particle coincidence measurements. An event was considered valid only if a particle and a γ-ray detection occurred within a ~500 ns time window. Because the response time of the HPGe detectors is much larger than that of the phoswich detectors, in order to verify coincidence before the charge-to-digital conversion, one would have to insert a delay of several times the value of the particle pulse rise-time, degrading the information contained in the pulse shape. Therefore, the digital conversion of the particle information is initiated promptly, and the coincidence with the γ rays is verified later. When no γ rays are detected, this conversion is aborted, allowing new events to be processed by the electronic modules. Each registered event contains the energy loss (Δ*E*) and residual energy (*E*) of the charged particle, and energy and time (relative to the particle detection) information of each γ ray (for further details see Ref. [3]). The measurements at each beam energy were divided in various runs (about 3 or 4 h each) to check for gain variations. The run was changed when the peak referring to the $2^+ \rightarrow 0^+$ transition of ^{110}Pd reached around 1–5 × 10^5 counts.

3. Data reduction

The first step in obtaining the cross-sections before extraction of the peak areas was to create gain corrected γ-ray spectra (in the region between 0 and 2500 keV). The calibration was performed using the γ-ray transition energies of ^{110}Pd (E_γ=373.8 keV) and ^{28}Si (E_γ=1779 keV, formed from the reaction of the beam with ^{16}O target contamination), both corresponding to $2^+ \rightarrow 0^+$ transitions. The final energy dispersion was chosen to be 1 keV per channel (Fig. 2).

New γ-ray spectra were obtained for each pair combination of a HPGe detector and a particle detector, selecting only data correlated with the ^{18}O cut of the ΔE–E plastic phoswich scintillator bi-parametric spectrum (Fig. 3). The ^{18}O particles are expected to be concentrated in a nearly vertical slice because at this energy the scattered particles did not have enough energy to reach the E detector. Fig. 4 shows an example of a γ-ray spectrum from detector G1 in coincidence with C3. Note the peak/background enhancement in comparison to Fig. 2.

The following step consisted in subtracting the background (due mainly to Compton scattering and to chance coincidences) of the spectra. To do this, it was necessary to select one peak and two background regions (or gates) in each of the spectra. The peak regions of the γ-ray and time spectra (represented by P and T, respectively) contain contributions from proper (or clean) events (photopeak p, and truly correlated coincidences t, respectively) as well as background events (Compton b, and chance coincidences c, respectively). The background regions (chosen on both sides in the neighborhood of the peaks), however, are supposed to contain only background events (B, Compton events, and C, chance coincidence events). An example of these regions can be seen in Figs. 4 and 5.

One can define, for the corresponding sets of events, the following algebraic relations (the plus sign signifying the union of the sets):

$$P = (p+b) \quad \text{and} \quad T = (t+c) \tag{1}$$

The events which are selected by both the γ-ray and time peak gates (P and T, respectively) correspond to the intersection (represented algebraically by the product) of those sets

$$PT = (p+b)\cdot(t+c) = pt + bt + pc + bc \tag{2}$$

Considering the background gated event sets (B and C) to be statistically similar to the b and c event sets, one can write, for the histogram $H[S]$ extracted from set S (*i.e.* a spectrum, either mono- or bi-parametric, *e.g.* $H(E, \Delta E)$, with the arguments measured in channels): $H[b] \approx \alpha H[B]$ and $H[c] \approx \beta H[C]$, where $\alpha = N_b/N_B$ and $\beta = N_c/N_C$ are numerical normalization factors taking into account the different number of elements (events) N_i of each set (typically due to the different gate widths in the number of channels). These numbers can be obtained by the evaluation of the corresponding areas in the respective spectra (Figs. 4 and 5). From these expressions, the clean histogram $H[pt]$ can be approximated by the background subtracted histogram

$$H[pt] \approx H[PT] - \alpha H[BT] - \beta H[PC] + \alpha\beta H[BC] \tag{3}$$

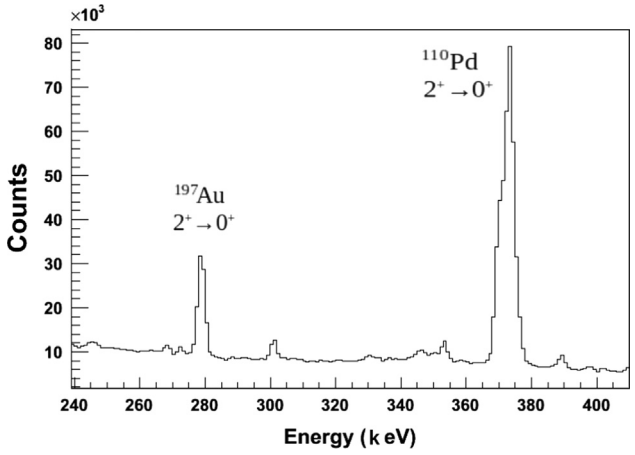

Fig. 2. Calibrated detector G1 γ-ray spectrum of the ^{18}O+^{110}Pd at 53.6 MeV showing the $2^+ \rightarrow 0^+$ transition of ^{110}Pd (E_γ=373.8 keV) and the $5/2^+ \rightarrow 3/2^+$ transition of ^{197}Au (E_γ=279.0 keV).

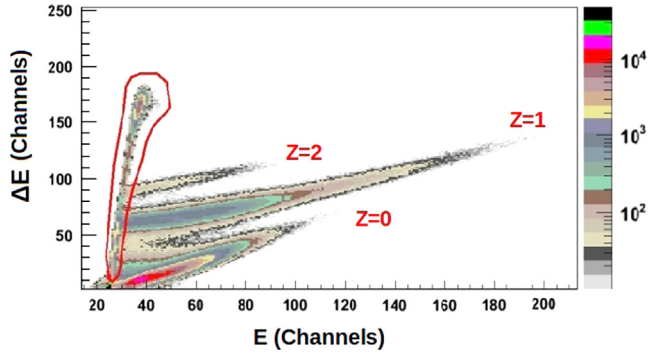

Fig. 3. Typical ΔE–E spectrum obtained in the experiment. This is the spectrum measured with the phoswich scintillator placed at 53° with relation to the beam (C3). The beam energy used in the reaction was 53.6 MeV. The red line delimits the cut where ^{18}O is expected in the spectrum. At this energy the scattered ^{18}O particles did not have enough energy to reach the E detector. The bands for particles with charge equal to 0, 1 or 2 are also indicated in the figure. (For interpretation of the references to color in this figure caption, the reader is referred to the web version of this paper.)

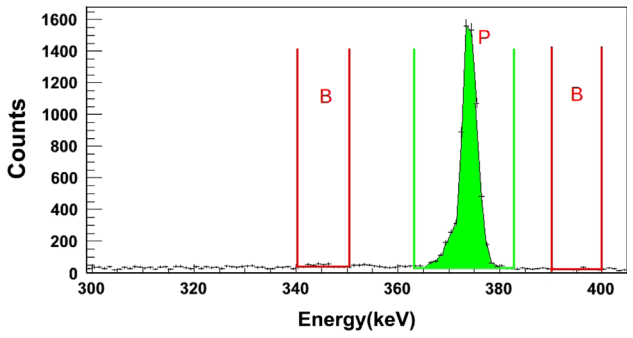

Fig. 4. A calibrated γ-ray spectrum showing the transition $2^+ \rightarrow 0^+$ of ^{110}Pd (E_γ=373.8 keV). The beam energy was of 53.6 MeV and this is the γ-ray detector G1. Note the peak to background ratio improvement compared to that of Fig. 2. The red regions (B) delimit the background that will be subtracted from the peak delimited by the green region (P). (For interpretation of the references to color in this figure caption, the reader is referred to the web version of this paper.)

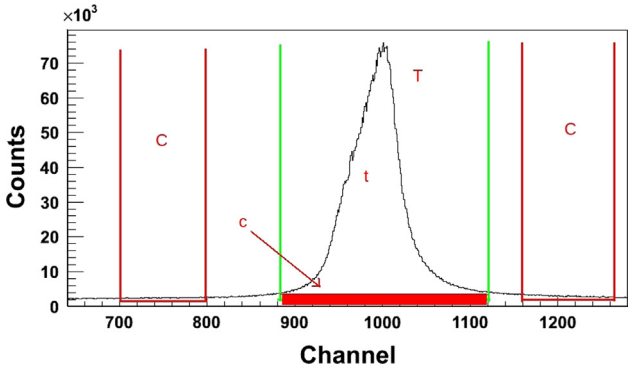

Fig. 5. Time spectrum showing the peak region (T) and the background regions (C). The long tail on the right side of the prompt peak in this total projection spectrum is due to delayed coincidence events, *e.g.* from γ decay of isomeric states populated by fusion evaporation reactions, target activation, neutron events, etc. The tail is absent when the time spectrum is gated by the scattered charged particle and by a specific γ-ray transition from a short lived state.

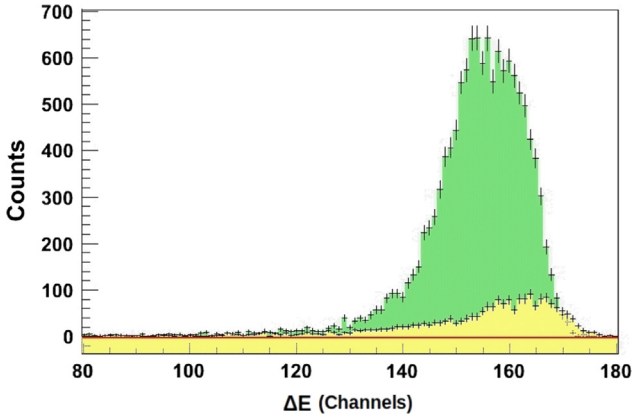

Fig. 6. Typical ΔE–E spectrum projected in the ΔE axis. This is the spectrum measured with the phoswich scintillator C5. The beam energy used in the reaction was 53.6 MeV. The green region corresponds to the $2^+ \rightarrow 0^+$ transition of ^{110}Pd and the yellow region corresponds to transition $5/2^+ \rightarrow 3/2^+$ of ^{197}Au (target backing). (For interpretation of the references to color in this figure caption, the reader is referred to the web version of this paper.)

The final step consisted in projecting the new ΔE–E spectra on the ΔE axis. The new spectra obtained after this procedure present negligible background (see Fig. 6). The differential cross-section and the angular distribution can be obtained from the peak areas of these spectra.

Fig. 6 demonstrates that this method can separate two different nuclear species (^{110}Pd and ^{197}Au) by choosing the proper gates in the γ-ray spectrum, even if the particle events were in the same particle cut (in this case, the ^{18}O particle). Unfortunately, if two transitions have very similar γ-ray energies it is impossible to distinguish between them. In this experiment, this happened in the case of the $4^+ \rightarrow 2^+$ transition in ^{110}Pd and $7/2^+ \rightarrow 3/2^+$ of ^{197}Au, making it impossible to study the angular distribution of the 4^+ state of ^{110}Pd.

4. Cross-section calculation

Defining experimental yield (Y) as the number of counts of a γ-ray peak divided by its detection efficiency, it is possible to correlate Y with the differential cross-section. A reference measurement of a low beam energy (E_{ref}) (below or near the Coulomb barrier, E_{bar}=46.6 MeV in the present case) is used to normalize the data taken at higher energies. The differential cross-section at E_{ref} is assumed to be known (a nearly pure Coulomb excitation differential cross-section). In addition a reference low scattering angle (θ_{ref}) measurement is used as normalization for larger angles, considering that, at this angle, a nearly pure Coulomb excitation occurs.

The theoretical yield can be expressed as $Y = I(E)N\ \Delta t[\int_{\Delta\Omega_{p,\gamma}} (d^2\sigma/d\Omega_p\, d\Omega_\gamma)\, d\Omega_p\, d\Omega_\gamma]$, where $I(E)$ is the beam current for a specific beam energy E, N is the areal density of nuclei in the target, Δt is the time duration of the experiment, and $\Delta\Omega_i$ are the solid angles for the particle (i=p) and γ-ray (i=γ) detectors. Cancellation of the parameters $I(E)$, N and Δt by taking ratios of yields is convenient in order to avoid systematic errors.

Since the particle inelastic scattering and the subsequent γ decay are decoupled (due to the wide difference in time-scales), it is possible to write

$$\frac{d^2\sigma}{d\Omega_p\, d\Omega_\gamma} = \frac{d\sigma}{d\Omega_p}(E,\theta_p) W(E,\theta_\gamma,\theta_p,\phi_{\gamma p}) f_u f_b \tag{4}$$

where $(d\sigma/d\Omega_p)(E,\theta_p)$ is the differential cross-section as a function of the particle scattering angle, $\phi_{\gamma p} = \phi_\gamma - \phi_p$ is the polar angle difference between the γ ray and particle directions, $W(E,\theta_\gamma, \theta_p,\phi_{\gamma p})$ manifests the γ-ray anisotropy (we define this function, which is normalized to 1 when integrated in all directions θ_γ, ϕ_p, as the "Directional Emission Probability" or DEP), f_u is the upper level feeding, and f_b is the decay branching correction factors. The DEP is the probability per unit of solid angle (probability density) that the γ ray, if emitted, is directed towards $(\theta_\gamma,\phi_\gamma)$ in coincidence with the particle emitted within $d\Omega_p$ around (θ_p,ϕ_p). The factor f_b is obtained from known parameters governing γ decay from the level in question; f_u is known from previous measurement or may be evaluated theoretically.

The expression for the DEP is [2]

$$W(E,\theta_\gamma,\theta_p,\phi_{\gamma p}) = \frac{N}{\sqrt{4\pi}} \sum_{\lambda q} \sqrt{\frac{2I+1}{2\lambda+1}} \rho_{\lambda q}(E,\theta_p) A_\lambda(\delta) Y^*_{\lambda q}(\theta_\gamma,\phi_{\gamma p}) \tag{5}$$

In this sum, λ runs over even integer values (due to parity conservation) such that $0 \le \lambda \le 2I$ and $0 \le \lambda \le L+L'$, where I is the angular momentum of the γ-ray parent state, and L, L' are the multipolarities (with mixing ratio δ) of the γ transition, and $-\lambda \le q \le \lambda$. The normalization constant N ensures that $\int_{4\pi} W(\theta_\gamma, \theta_p)\, d\Omega_\gamma = 1$ (where we simplified the notation for the DEP, with the E and $\phi_{\gamma p}$ variables implicitly understood).

The (spherical) statistical tensor $\rho_{\lambda q}(E,\theta_p)$ [4] of the parent level is obtained from the scattering amplitudes $f_{MmM'm'}(\theta_p)$ (where M, m, M', and m' are angular momentum projections of target and projectile) calculated with the coupled channel (CC) code FRESCO [5], and $A_\lambda(\delta)$ is the multipole transition coefficient. Lastly, $Y_{\lambda q}$ is the spherical harmonic function. From now on, we define the symbol $W'(E,\theta_\gamma,\theta_p,\phi_{\gamma p})$ as the short form of the product $W(E,\theta_\gamma, \theta_p,\phi_{\gamma p}) \cdot f_u \cdot f_b$.

Defining the following expressions:

$$R_Y = \frac{Y(E,\theta_p)}{Y(E_{ref},\theta_p)} \div \frac{Y(E,\theta_p^{ref})}{Y(E_{ref},\theta_p^{ref})}$$

$$R_\sigma = \frac{d\sigma}{d\Omega_p}(E,\theta_p^{ref}) \frac{\frac{d\sigma}{d\Omega_p}(E_{ref},\theta_p)}{\frac{d\sigma}{d\Omega_p}(E_{ref},\theta_p^{ref})} \quad \text{and}$$

$$R_{W'} = \frac{W'(E,\theta_p^{ref})}{W'(E_{ref},\theta_p^{ref})} \div \frac{W'(E,\theta_p)}{W'(E_{ref},\theta_p)} \tag{6}$$

where E_{ref} is the reference energy and the reference angle is denoted by θ_p^{ref}. One may notice that R_Y depends on the experimentally measured quantities, while R_σ and $R_{W'}$ depend solely on a theoretical calculation. From Eqs. (6) it is possible to find that

$$\frac{d\sigma}{d\Omega_p}(E,\theta_p) = R_Y R_\sigma R_{W'} \tag{7}$$

It is important to mention that the reference differential cross-sections used were calculated with the code FRESCO, because it allows consideration of the Coulomb and nuclear parts in the potential. After obtaining the differential cross-sections for each γ-ray detector, an uncertainty weighted average was calculated as the final cross-section.

To calculate the $W(\theta_\gamma,\theta_p)$ factor, some input must be provided for a developed $C++$ code, designated as DEPCalc. One necessary input is the scattering amplitude of each state which was obtained as an output of coupled channel code FRESCO. From these amplitudes it is possible to obtain the statistical tensors.

Other inputs for DEPCalc were the positions of the detectors (HPGe and phoswich scintillators), the beam energy, the thickness and stopping power coefficients of the target (using these last three parameters made it possible to integrate $W(\theta_\gamma,\theta_p)$ over energy) and the geometric parameters of the collimators (allowing the angular integration of $W(\theta_\gamma,\theta_p)$). The ground and excited level

properties of the projectile and target were also inputs for the program, as well as the allowed transitions and their respective intensities. These inputs are used to calculate the feeding of each state. In this work the 2^+ state is fed by the excited states $2(2)^+$, 4^+ and $0(2)^+$. This effect was taken into account by considering the modifications that the inclusion of these indirect feedings make in the statistical tensor of the $2^+ \rightarrow 0^+$ transition. Other effects considered in the calculation of $W(\theta_\gamma, \theta_p)$ are the finite size of the γ-detector and the nuclear vacuum de-orientation effect. Both corrections are attenuation factors included in each multipole of the angular distribution; the first one was obtained using the Coulomb excitation code GOSIA. The second correction depends on the average hyperfine magnetic field in vacuum $\overline{H} = KZ(\nu/c)^x$ [2], where Z is the atomic number and ν is the recoil velocity of the nucleus. The parameters K and x were adjusted in a way that will be explained in Section 5.

5. Studies of $W(\theta_\gamma, \theta_p)$, determination of vacuum de-alignment parameters and incorporation of the corrections in the differential cross-section

5.1. The dependence of $W(E, \theta_\gamma, \theta_p)$ on the beam energy

The first study made was on the variation of the $W(E, \theta_\gamma, \theta_p)$ factor as a function of the incident beam energy. Fig. 7 demonstrates that, for a variation of 12 MeV in the incident beam energy, the variation of the DEP is quite small (at most 5% for G1 in coincidence with C1).

As said before, the $W(\theta_\gamma, \theta_p)$ was calculated theoretically with program DEPCalc. This variation can be experimentally tested by considering the yield ratio between the γ-ray detectors G1 and G2. Dividing the yield of detector G2 by the yield of detector G1 it is easy to find that

$$\frac{Y(E, \theta_\gamma^2, \theta_p)}{Y(E, \theta_\gamma^1, \theta_p)} = \frac{W(E, \theta_\gamma^2, \theta_p)}{W(E, \theta_\gamma^1, \theta_p)} \quad (8)$$

Fig. 8 shows the relative variation of these yield ratios with respect to their mean value for some particle detectors (C4, C5, C7, and C9), compared to their theoretical calculations. As can be seen again in this figure, the experimental yield ratios for different

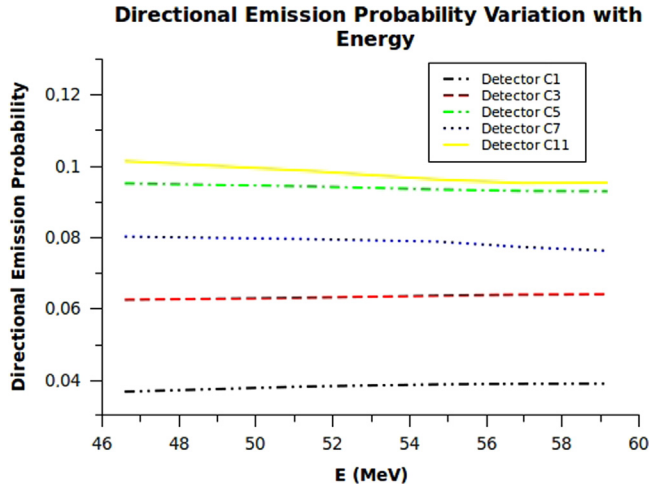

Fig. 7. Directional Emission Probability calculated for different particle detectors as a function of the incident beam energy. The solid yellow line represents the direction of detector C11, the blue dotted line the direction of detector C7, the green dashed and dotted line the direction of detector C5, the red dashed line the direction of detector C3 and the black dashed and double dotted line the direction of detector C1. (For interpretation of the references to color in this figure caption, the reader is referred to the web version of this paper.)

angles do not vary significantly with energy (considering the uncertainties), corroborating the results expressed in Fig. 7.

5.2. Analysis of the γ-ray anisotropy

Due to the manual assemblage of the collimators, a small displacement of the aperture positions can occur. A 2 mm displacement represents a $\pm 4^\circ$ variation in the polar (θ) or azimuthal (ϕ) angles. These displacements constitute possible systematic errors which have to be incorporated in the uncertainties of each experimental point. The procedure to evaluate the uncertainties consisted in calculating the theoretical differences between displaced and undisplaced yield ratios, for polar and azimuthal displacements separately. The results were then quadratically summed with the statistical uncertainty to obtain the final uncertainty at each point.

The systematic uncertainty due to a possible geometric displacement contributes much more (one order of magnitude in most cases) than the statistical uncertainty as can be seen by the relative uncertainties in all particle detector angles shown in Table 3. This fact was expected since the measurements were done for a long time, so, there were a lot of events for each angle, contributing for a very small statistical error.

Fig. 9 presents the γ yield ratios for each particle detector compared to the theoretical predictions. The yield ratios presented in Fig. 9 were also used to adjust the K and x factors of the vacuum de-alignment effect. The best fit values are $K = 10^{-7}$ and $x = 0.3$. Upper limits of $K < 10^{-6}$ and $x < 0.6$ were established for these factors.

The vacuum de-alignment, as well as any other attenuation effect (*e.g.* angular spread within the detector aperture angles), tends to flatten the γ-ray angular distribution and approximate the yield ratios to 1 and, therefore, reduce the DEP corrections to be applied later to the cross-section evaluations.

The reasonably good agreement between the data and the theoretical predictions (shown in Fig. 9, except, perhaps, for the largest charged particle detector angle at $\sim 140^\circ$) indicates that the model adequately accounts for the γ-ray anisotropy. This result corroborates the use of the model calculations in the DEP corrections applied to improve the accuracy of the cross-section evaluations (to be presented in Section 6). We would like to point out that the calculated anisotropy is not strongly dependent on details of the model. Indeed, various preliminary calculations were performed in the course of this work, *e.g.* with the inclusion of more or less inelastic channels, without major effects on the yield ratio predictions. Also, turning off the nuclear interaction while keeping the electromagnetic one (pure Coulomb excitation) changes the DEP by a very small amount, but has a major effect on the calculated inelastic excitation cross-section values. The normalization procedure (Section 4) adopted further reduces the model dependency of the cross-section measurements, since the γ-ray yield ratios depend weakly on the energy (see Section 5.1).

These yield ratio measurements constitute, therefore, a preliminary test of the theoretical model. If the model does not pass this test (which could happen in more complex situations), it has to be revised before being used to calculate the DEP corrections to be applied later. In principle, one could compare directly the calculated twofold differential cross-section $\left(d^2\sigma/d\Omega_p\, d\Omega_\gamma\right)$ with the experimental data. This is an interesting approach which can be proposed for more detailed future investigations of nuclear reactions by the particle–γ coincidence technique. Unfortunately, in our case, the large uncertainty in the scattering angle and the limited number of γ-ray detector angular positions prevent an accurate and extensive investigation of the γ-ray distribution function. The γ-ray angular correlation and the charged particle angular distribution have a different physical significance and, in

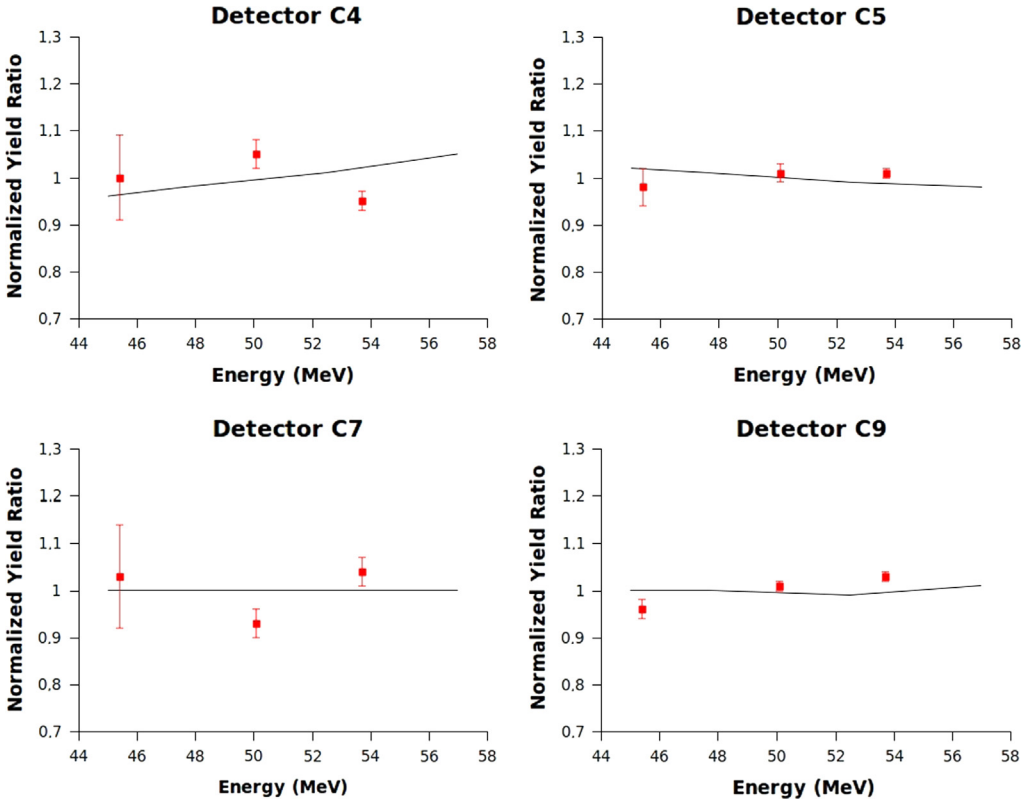

Fig. 8. The experimental yield ratios (normalized to their mean value) for particle detector C4, C5, C7, and C9 for the incident beam energies of 45.4, 50.1 and 53.6 are presented in red, while the black lines are the theoretical values. (For interpretation of the references to color in this figure caption, the reader is referred to the web version of this paper.)

Table 3
Table showing that the systematic relative uncertainty is much greater than the statistical one, except at 116.8°.

Angle (°)	Statistical uncertainty	Systematic uncertainty	Total uncertainty
34.8	4.4	10.1	11.0
50.2	3.6	14.6	15.1
61.1	3.0	64.7	64.8
73.7	2.2	40.5	40.5
80.8	2.4	14.8	15.0
108.6	3.3	6.0	6.8
116.8	12.2	8.1	14.6
125.6	1.1	10.0	10.1
135.0	1.2	10.1	10.2
143.0	1.5	9.1	9.2

the present case, a very different parametric sensitivity from the calculations. The DEP is sensitive to the electromagnetic properties of the excited states, angular momentum couplings and kinematics. It is important to note that the DEP is connected to the angular correlation, but it is normalized to 1 after the charged particle detection condition. Therefore the angular correlation is directly affected by the scattering cross-section, but the DEP is not. It turned out, in our case, that the calculated DEP is not sensitive to the nucleus–nucleus potential and channel couplings, but the cross-sections, of course, are strongly affected by those.

5.3. *Importance of the various effects on the angular distribution*

Prior to making the study of corrections to our calculations and how these effects alter the differential cross-section, a few data points had to be discarded. For angles close to 90°, displacements in the peaks of the ΔE–E spectra was noticed. This displacement is due to the fact that, for these angles, the scattered ^{18}O measured by ΔE–E detectors has to travel across a larger distance inside the target compared to other scattering angles. As a consequence, the energy loss of these particles is not negligible (over 20 MeV for 80.4° for example) and a large portion of the measured peak is lost. For this reason the detectors C6, C7 and C8 had their values disregarded in the angular distributions.

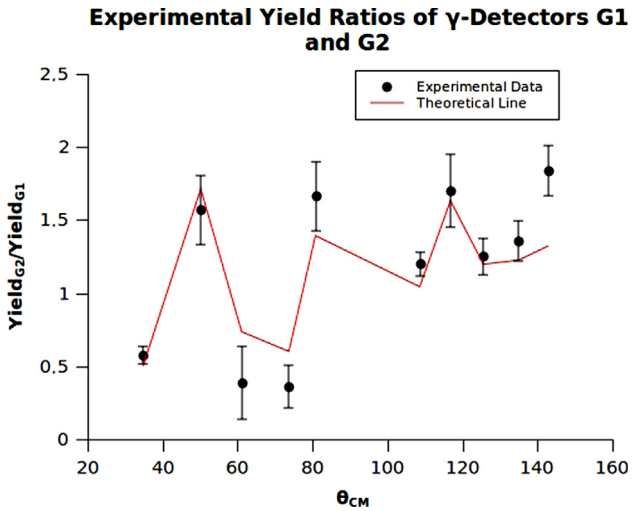

Fig. 9. Experimental yield ratios for the ten different particle detector angles at a beam energy of 53.6 MeV. In this figure the solid red line represents the ratios obtained from the DEP calculation for the incident beam energy of 53.6 MeV with no displacement. The experimental total uncertainties consider the angular uncertainties due to a possible 4° displacement in the polar (θ) and azimuthal (ϕ) angles. (For interpretation of the references to color in this figure caption, the reader is referred to the web version of this paper.)

The data at the beam energy of 50.1 MeV were used to normalize the data at 53.6 MeV. The reason for this was the low statistics of the data at 45.4 MeV. The corrections that were studied (how their incorporation into $W(\theta_\gamma,\theta_p)$ calculation affects the differential cross-section obtained) were the energy integration over the energy loss in the target; the angle integration over the face of the particle detectors; the finite size of the γ-ray detectors; the size of the beam spot on the target and the vacuum de-alignment. It was observed that the most significant effect that could alter the angular distribution is the finite size of the γ-ray detectors, as can be seen in Table 4. In Fig. 10, the corrected angular distribution curve considering only this effect is presented. Even for this effect, the obtained differential cross-sections are only slightly modified. This can be explained by the fact that the differential cross-sections are obtained from yield ratios. In these ratios, the incorporated corrections alter both detector yields in a similar manner. The curves which take into account each of the other effects separately would be intermediate between this and the no-corrections curve, and were, therefore, not presented, for clarity.

Table 4 gives the percentage variation of the differential cross-section due to the incorporation of each correction solely for detector C11 (the detector that was most affected by the corrections). These variations were obtained by including in the calculations only one correction at a time, disregarding all the others. The analysis of this table shows that the γ detector finite size and the vacuum de-alignment corrections are the two that most alter the angular distribution. One interesting aspect that was noticed is that if both corrections are included at the same time in the calculations the behavior of the angular distribution is the same as that obtained if only the γ detector finite size effect is included. An explanation for this is that as the γ detector finite size effect flattens the initial angular anisotropy of the γ-ray decay, the other effect becomes imperceptible.

The analysis of Fig. 9 allows us to deduce that the method developed is useful to identify different reaction mechanisms, since if the reaction mechanism employed to generate the DEP calculation was wrong, the good agreement of theory and experimental data observed in Fig. 9 would be unlikely. From Fig. 10 it is possible to say that the method may be used to obtain angular distributions.

Table 4
Table showing the relative variation that the incorporation of each effect makes to the cross-section for the detector C11.

Correction applied	Relative variation (%)
Energy integration	0.55(4)
Angular integration	3.70(4)
γ detector finite size	21.98(5)
Beam spot size	3.43(4)
Vacuum de-alignment	14.31(4)

6. The angular distributions

The next step consists in comparing the extracted angular distributions with theoretical results calculated with code FRESCO. The scattering potential considered to make the theoretical calculations consists of a sum of a Coulomb potential plus a nuclear potential. This nuclear potential consists of two parts, the real one is given by the *São Paulo Potential* (PSP) while the imaginary nuclear potential is given by the Woods–Saxon form $W(r) = -100/(1+e^{(r-1.06)/0.2})$ MeV (known to adequately take into account the compound nucleus formation [6,9]). The first four excited states of ^{110}Pd (2^+, $2^+(2)$, 4^+ and $0^+(2)$, and the first excited state of ^{18}O (2^+) were coupled in the calculations. The comparison between the theoretical and measured data can be seen in Fig. 11. A similar calculation model (which, in addition, includes transfer couplings) was successful in the description of the quasi-elastic, inelastic, and transfer excitation function data for this system [6,8].

It is important to mention that the theoretical angular distributions take into account the upper level feeding of the ^{110}Pd $2^+ \rightarrow 0^+$ transition from the $2^+(2)$, 4^+ and $0^+(2)$ and their respective transition intensities. For forward angles this contribution is very small ($\sim$ 1%); however, for large scattering angles the upper level feeding contribution can be about 30%.

The data obtained for each experimental point consist of an integration of the cross-section over the angular aperture of the ΔE–E detector collimator. As can be seen from Table 2 this aperture is small for low scattering angles, however, it cannot be ignored for large scattering angles, so, it is necessary to correct the

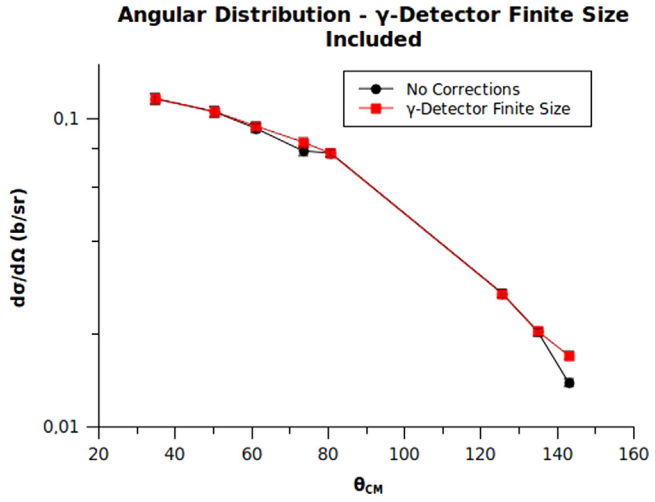

Fig. 10. Angular distribution for the incident beam energy of 53.6 MeV. In this case the correction of γ detector finite size effect is applied to the angular distribution of γ rays (red). The black points represent the case when no corrections are applied to the angular distribution of γ rays. (For interpretation of the references to color in this figure caption, the reader is referred to the web version of this paper.)

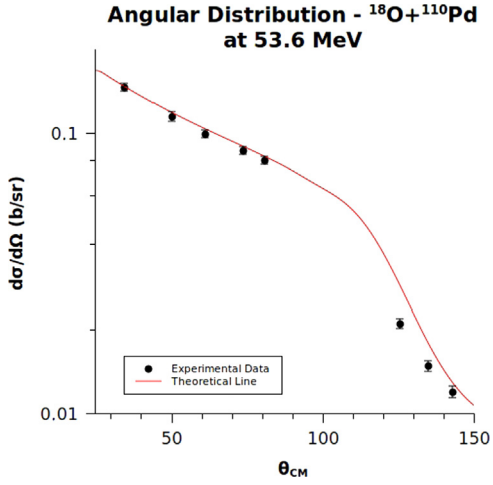

Fig. 11. Angular distribution for the incident beam energy of 53.6 MeV. The black points are the experimental data with all the corrections considered applied to the angular distribution of γ rays. The red line is the theoretical prediction made with CC code FRESCO (see text). The smallest angle data point ($\theta_{pref} = 30^\circ$) is used for normalization. (For interpretation of the references to color in this figure caption, the reader is referred to the web version of this paper.)

data of detectors C9, C10 and C11. The procedure to correct these data consisted in comparing the average theoretical differential cross-section over the detector solid angle with the theoretical differential cross-section at the central point, obtaining a correction factor.

From an analysis of Fig. 11 one can see that the theoretical angular distribution for wide scattering angles is systematically above the experimental data. This result is expected since the CC calculations made do not consider the transfer channels (such as 1n, 2n and α particle transfer). These transfer channels probably will reduce the values of the differential cross-sections for large scattering angles.

The data for 2 neutron transfer is still under analysis and will be presented in a future paper.

7. Conclusions

The measurement of γ-particle coincidences using the γ spectrometer Saci-Perere (LAFN-IFUSP-DFN) was successfully performed and the angular distribution for the 2^+ excited state of ^{110}Pd was obtained.

The normalization procedure adopted reduces various possible systematic uncertainties which affect the cross-section evaluations by the γ-particle technique. We conclude that a solid method to analyze the data and identify the reaction mechanism was developed and can be now employed to obtain the angular distributions of other nuclear systems.

From Fig. 11 it is possible to deduce that the theoretical calculations made fit the data reasonably well, except for large scattering angles, presumably due to the lack of transfer channels in the calculations.

The study of other systems, such as ^{9}Be+^{120}Sn, ^{6,7}Li+^{120}Sn, ^{10}B+^{27}Al and ^{6}Li+^{154}Sm, has been initiated with a redesigned collimator system optimized for lighter beams.

Acknowledgments

This work was supported by FAPESP, Cnpq and CAPES, Brazil.

References

[1] J.A. Alcántara-Núñez, J.R.B. Oliveira, et al., Nuclear Instruments and Methods in Physics Research Section A 497 (2003) 429.
[2] T. Czosnyka, D. Cline, C.Y. Wu, Bulletin of the American Physical Society 28 (1983) 745.
[3] V.A.B. Zagatto, Dissertação de Mestrado, Universidade de São Paulo, IFUSP, 2011 (online version: 〈http://www.teses.usp.br/teses/disponiveis/43/43134/tde-26042012-195616/pt-br.php〉).
[4] R.D. Gill, Gamma-Ray Angular Correlations, Academic Press, New York, 1975.
[5] I.J. Thompson, Computer Physics Reports 7 (1988) 167.
[6] D. Pereira, et al., Physical Review C 74 (2006) 034608.
[8] J.R.B. Oliveira, et al., in: Proceedings of XVIII International School on Nuclear Physics, Neutron Physics and Applications, Varna, Bulgaria, 21–27 September 2009.
[9] D. Pereira, C.P. Silva, J. Lubian, E.S. Rossi , L.C. Chamon, Physical Review C 73 (2006) 014601.